THE JOURNAL OF PHYSICAL CHEMISTRY B

Article

pubs.acs.org/JPCB

Local Structure Evolution and its Connection to Thermodynamic and Transport Properties of 1-Butyl-3-methylimidazolium Tetrafluoroborate and Water Mixtures by Molecular Dynamics Simulations

Xiujuan Zhong, Zhen Fan, Zhiping Liu,* and Dapeng Cao*

Division of Molecular and Materials Simulation, State Key Laboratory of Organic−Inorganic Composites, Beijing University of Chemical Technology, Beijing 100029, China

Supporting Information

ABSTRACT: Our recently developed improved united atom force field shows a good quality to reproduce both the static and transport properties of neat ionic liquids (ILs). Combined with the TIP4P-Ew water model, the force field is used to simulate the mixture of 1-butyl-3-methylimidazolium tetrafluoroborate ([C_4mim][BF_4]) and water without further optimization to adjust any cross parameters. Liquid densities of the mixture are well predicted over the entire concentration range at temperatures from 298.15 to 353.15 K. Simulations also reproduce the positive values of excess volumes and excess enthalpies, as well as their increase with temperature. The simulated viscosities are in good agreement with experimental values, especially in the water-rich region. We found three distinct regions by analyzing the concentration dependent self-diffusion coefficients via Stokes−Einstein (SE) relation, indicating the mixture experiences significant microheterogeneity with the adding of water. This observation is well connected to the structure features obtained in simulations, such as radial distribution functions (RDFs), spatial distribution functions (SDFs) and water clustering analysis. At the water mole fraction (x_2) less than 0.2, most of the water molecules are isolated in the polar cation−anion network in ionic liquids. With the increase of x_2 from 0.2 to 0.8, large water cluster forms and eventually percolates the whole system. When x_2 > 0.8, ionic liquids show a moderate degree of aggregation (with maximum around 0.9 to 0.95) before the cations and anions are fully dissolved in water.

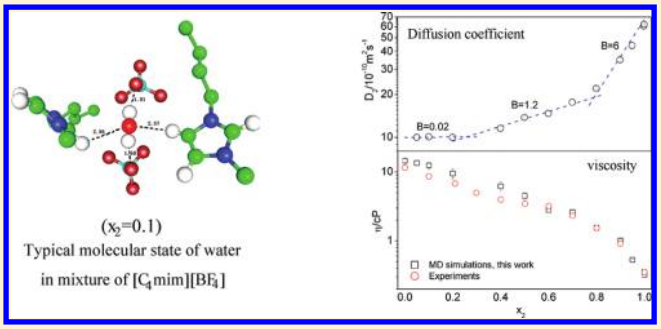

1. INTRODUCTION

Ionic liquids (ILs) are room temperature molten salts which consist of large organic cations (typically bulky and asymmetric) and inorganic or organic anions. These liquids have attracted a great deal of attention in recent years due to their unique properties, such as negligible vapor pressure, good thermal stability and highly tunable properties.[1] It is well-known that water is the most common contaminator in ILs due to their hygroscopic nature, even for those considered "hydrophobic". The intruding of water induces disturbing of microscopic structure in the IL, in other words, the local environment that molecules can "feel". As a result, significant change of various properties is found when adding water to ILs,[2] such as the surface tensions, diffusion coefficients, viscosities and conductivities, as well as the rates of chemical reactions.[3] Therefore, it is very important to investigate the behavior of the mixture of ILs and water, not only because water is inevitable in any practical applications of ILs, but also because it provides new opportunity to tune the properties of ILs by adding other small molecules like water.

Various experimental techniques, such as small-angle neutron scattering (SANS),[4−6] NMR,[6−12] IR/Raman[13−25] and fluorescence correlation spectroscopy (FCS),[26] were used successfully to probe the structure and dynamics of IL-water mixtures, providing valuable information on the microenvironment of both water and cations/anions. It was elucidated by many investigations[8,14,19,22,24] that the interaction between anion and water plays the major role when small amount of water is absorbed in IL, indicated by the structure of isolated water molecule bounded to two anions via hydrogen bonds. As the concentration of water increases, water molecules began to form dimers, as well as larger clusters,[18,24] Thus, the polar network established by strong electrostatic interactions between cations and anions is disrupted gradually. When more and more water is added, IL is dissolved in water just like any conventional electrolyte. However, the surfactant-like behavior is typically found for most of ILs before they are fully dissolved in water, as expected due to their amphiphilic molecular structures.

Received: January 5, 2012
Revised: February 20, 2012
Published: February 21, 2012

   dx.doi.org/10.1021/jp3001543 | J. Phys. Chem. B 2012, 116, 3249−3263

As an important complement to the experiments, molecular simulation is a powerful tool in studying the behavior of solutions. The atomistic detailed information can be obtained explicitly in simulations, through which various thermodynamic and transport properties can be calculated.

After the pioneered work of simulations of the mixtures of dimethylimidazolium ([C_1mim]) ILs and water by Lynden-Bell group,[27] various properties were investigated for ILs/water mixtures by molecular simulations at different levels. Among them, both static quantum chemistry (QC) calculation[13,15,28] and density functional theory (DFT) based ab intio molecular dynamics (AIMD),[29−31] although providing invaluable information that can not be accessed by other methods, are highly computationally demanding. Therefore, they are limited to study relative small systems of several tens to hundred atoms and very short time dynamical behavior of a few ps.

The atomistic-level molecular dynamics (MD) is widely used to study the structure, dynamics and phase behavior of aqueous IL solutions.[30,35−43] For example, Wipff and co-workers investigated the aqueous interface of hydrophobic ILs,[37,38] and discussed the potential application to the extraction of metal ions.[32] Schröder et al. discussed the network between different species and dielectric spectra in [C_4mim][BF_4]/water mixture.[33−35] Maginn et al. simulated various thermodynamic and transport properties of aqueous ILs, including excess molar volumes and viscosities.[36−38] Voth et al. investigated the nanostructural organization in IL/water mixtures.[39] They also discussed the effects of tail length and anion on dynamics and structure.[40] Margulis et al. simulated the effect of water on the fluorescence spectra in [C_6mim][PF_6].[41] Porter et al. simulated a water-miscible and a water-immiscible ILs when mixed with small quantities of water.[42] Picalek et al. studied the concentration dependent surface tensions of aqueous [C_4mim][BF_4] and discussed the effect of adding polarization into the force fields.[43] Raju and Balasubramanian analyzed the distribution of potential energies in [C_4mim][PF_6] with small amount of water.[44] Klahn et al. proposed a straightforward and computationally inexpensive method to predict the miscibility between ILs and water via their simulation results.[45] English et al. investigated the response of the external electromagnetic field effect of IL/mixture by nonequilibrium MD.[46] Lopes et al. performed a comprehensive study of the liquid−liquid equilibria between water and isomeric pyridinium-based ILs by using a combination of experiments and simulations.[47] Migliorati et al. studied the thermal and structural properties of ethylammonium chloride/water mixture by X-ray powder diffraction, assisted by simulations.[48] Mendez-Morales et al. analyzed the influence of water concentration on the structure and dynamics of different IL/water mixtures.[49] Liu et al. estimated the Maxwell−Stefan diffusion coefficients of binary systems of [C_4mim]Cl and water from MD simulations.[50] Bhargava and Klein focused their simulations on the aggregation behavior of ILs in water uing both the all-atom and coarse grained (CG) models.[51,52] Recently, they also published an excellent review on the studies of IL/water mixture by computational methods at different levels (abundant results by experiments were also introduced).

Despite the active research on various properties of IL/water mixtures by MD simulations, relative few studies made sufficient quantitative comparisons between the simulated and experimental values covered the full range of concentration, i.e., including the water-rich and IL-rich regions. Moreno et al. simulated[11] the systems of [C_4mim][BF_4]/water in IL-rich region using two published force fields.[53,54] Both predict the mixture densities in good agreement with experiments, within a difference of 1%. However, the simulated excess molar volumes are negative, which disagrees the positive volume expansion upon mixing by experiments.[2] Kelkar et al.[36] studied the [C_2mim][$EtSO_4$]/water mixtures extensively by their established force field for neat ILs. They stressed that a minor error of density can greatly affect the values of excess molar volume, so the latter is a much more sensitive validation of force field in simulation of mixtures. Recently, Lopes and co-workers[55] focused on the energetics of the same system by using both the calorimetric experiments and MD simulations. They also analyzed the structure in detail by different aggregation state of water and ions captured in MD simulations[56] over entire concentration range for the mixture.

As it is well-known, the simulated results are heavily dependent on the engaged force field, in which the functional form and corresponding parameters are given to describe the interactions between atoms. Most of the early developed force fields,[53,54,57] although successfully reproduced some properties of IL very well, such as crystal structure and liquid density, were found to predict substantially slower dynamics of ILs.[58,59] In virtue of recent advance of experimental techniques, the heats of vaporization were reasonably determined by different methods (especially for the thermally stable [NTf_2] IL family),[60,61] which provides valuable source to validate the force field of ILs. Not surprisingly, most of the early developed force fields give significantly larger values of the heat of vaporization.[62] In addition, evidence is also shown overstructured ILs is obtained by the force field when compared with AIMD simulation results.[29,63,64] The most reasonable way to overcome this seems to introduce polarization explicitly, which was successfully done by Borodin and Smith for a wide range of cations and anions.[65,66] However, the polarizable force fields are more computationally costly and have fewer implements in simulation codes. Therefore, the classical force field without explicit inclusion of polarization is still dominatingly used in atomistic-level simulations at present.

Recently, we proposed a simple strategy[67] to include the polarization effect averagely by refitting the atom charges using ab initio results of ion pair dimers, in which we need not add any new functional forms into the force field, although it is necessary to adjust some parameters, such as van der Waals (vdW) diameter, and to refit the dihedral coefficients. It is an improvement followed the methods proposed earlier by Maginn[68] and Balasubramanian[69] groups. The atom charges fitted by ion pair dimer are more likely to resemble those in bulk liquid phase, compared with those by fitting single ion pair,[68] or just rescaling charges in the original nonpolarizable force field.[59] It is also less artificial than adjusting the atom charges to fit the structure and dynamics properties in liquid phase, either by AIMD simulations or experiments.[69]

Using the above method, we developed an improved classical united-atom (UA) force field for imidazolium-based ILs combined with a few common used anions,[62] by which the thermodynamic and transport properties of neat ILs are reproduced in good accuracy. Very recently, Rai and Maginn performed Gibbs ensemble Monte Carlo (GEMC) to study the vapor−liquid coexistence curves and critical points of ILs of [$C_n$mim][BF_4][70] and [$C_n$mim][NTf_2][71] using the force fields, in which very reasonable results were also obtained in comparison to the values extrapolated from low-temperature experiments. However, it is less clear how accurate the force field in predicating the properties of ILs mixtures. As mentioned above, two published force fields[53,54] failed to

dx.doi.org/10.1021/jp3001543 | J. Phys. Chem. B 2012, 116, 3249−3263

reproduce the positive volume change upon mixing [C_4mim][BF_4] and water.[11] This motivates us to investigate the system using our new proposed force field over the entire concentration range. We chose [C_4mim][BF_4]/water mixture because the system is extensively studied by using various methods and a large number of experimental results are available.[2,72−75] This work focuses on two subjects: (1) Make quantitative comparisons between the simulated and available experimental values, including liquid densities, excess volumes, excess enthalpies, self-diffusion coefficients and viscosities. (2) Investigate the local structural evolution of the mixture during the adding of water and its connection to various macroscopic properties.

2. MODELS AND SIMULATION METHODOLOGY

2.1. Force Fields. The interaction energy of [C_4mim][BF_4] is described by the standard classical functional form of the force field, in which the parameters are optimized for modeling the IL systems in our recent work,[62] given by

$$U = \sum_{bon\ ds} K_r(r - r_0)^2 + \sum_{angels} K_\theta(\theta - \theta_0)^2 + \sum_{dihed} K_\chi[1 + \cos(n\chi - \delta)] + \sum_{i<j} 4\varepsilon_{ij}\left[\left(\frac{\sigma_{ij}}{r_{ij}}\right)^{12} - \left(\frac{\sigma_{ij}}{r_{ij}}\right)^{6}\right] + \sum_{i<j} \frac{q_i q_j}{r_{ij}} \quad (1)$$

The first three terms represent bonded interactions, and the last two terms represent nonbonded interactions. K_r, K_θ, and K_χ are energy coefficients of the bonds, angles, and dihedrals, respectively; ε_{ij} and σ_{ij} are the energy and size parameters between atoms i and j in the Lennard-Jones (LJ) potential; and q_i is the charge on atom i. A scaling factor of 0.5 is applied to nonbonded parameters between atoms separated by three consecutive bonds (1−4 interactions). The TIP4P-Ew model[76] is adopted for water, which is a reparameterization of the standard TIP4P[77] model. The thermodynamic and transport properties of water are well reproduced by TIP4P-Ew at temperatures from 235 to 400 K, including a density maximum at ∼1 °C. All the parameters were collected in Table S1 in Supporting Information. The cross parameters for interactions between unlike species are obtained by the Lorentz−Berthelot (LB) combining rules without further adjustment.

2.1. Molecular Dynamics Simulation Details. The mixtures of [C_4mim][BF_4] (**1**)−water (**2**) were studied by molecular dynamics at ambient pressure and six temperatures ranging from 298.15 to 353.15 K. The mole fractions of water, x_2, are 0.0, 0.05, 0.1, 0.2, 0.4, 0.5, 0.6, 0.7, 0.8, 0.9, 0.95 and 1.0, as shown in Table 1. The smallest number of either component is chosen to be larger than 50 to get good statistics in simulations. Another four simulations of much larger systems (10 times the small systems) with x_2 = 0.2, 0.4, 0.6, and 0.8 at 298 K were performed to study the size effect on the simulated properties. As is shown in Table S2 and Figure S1, Supporting Information, the difference between the small and large size simulations is within the statistical uncertainty for properties discussed in this work, indicating the system sizes used in this work are large enough. To study the state of cations and anions fully dissolved in water, we also performed MD simulations of one single ion pair and 1000 water molecules at 298.15K. It was found that the cation and anion (staring from ion pair) are separated by water during simulation in a few tens ps.

Table 1. Number of Ion Pairs (N_1) and Water (N_2), Equilibrated Box Size (L_{box} at 298 K and 1 bar) by Simulation for a [C_4mim][BF_4] (1)−H_2O (2) Mixture[a]

N_1	N_2	L_{box}, nm	x_2	w_2, %	c_1, mol/L	c_2, mol/L
256	0	4.31205_{62}	0	0	5.304	0
950	50	6.68550_{127}	0.05	0.42	5.281	0.278
450	50	5.22110_{92}	0.1	0.88	5.252	0.584
260	65	4.36685_{90}	0.2	1.95	5.186	1.297
165	110	3.80125_{52}	0.4	5.04	4.990	3.327
140	140	3.63340_{38}	0.5	7.38	4.848	4.848
110	165	3.40075_{38}	0.6	10.7	4.646	6.969
81	189	3.14040_{40}	0.7	15.7	4.344	10.137
65	260	3.04160_{39}	0.8	24.2	3.837	15.349
50	450	3.07690_{40}	0.9	41.8	2.851	25.661
50	950	3.53430_{45}	0.95	60.2	1.881	35.745
0	512	2.48865_{23}	1	1	0	55.180

[a]Statistical uncertainty of L_{box} is shown in subscript. Concentrations at different units (mole fraction x, weight fraction w, and molarity c) are also listed for reference.

It is well-known that the dynamics in ILs are very slow. To avoid the possible initial state dependent simulation results, we performed an accelerated strategy including three steps: (1) the initial configuration was prepared by PACKMOL[78] in a cubic box which is about 20% larger than its "real" size. Heat the system to a higher temperature, typically 700 K for neat IL, at which NpT simulations were run for several hundreds of picoseconds to accelerate the dynamics and overcome possible energetic trapping. The system was then cooled down sequentially to the target temperature. (2) The final configuration from step 1 was equilibrated in NpT ensemble for 10 ns, and another 6 ns NpT run was performed to obtain ensemble averaged properties, such as intermolecular energies and liquid volumes. (3) Set the simulation box to the average volume obtained from the former NpT run. After 5 ns of equilibration, the system was run more than 40 ns in NVT ensemble to estimate the self-diffusion coefficients and shear viscosities. Considering the large computational cost of calculating the self-diffusion coefficients and shear viscosities in reliable accuracy by equilibrium MD,[79] especially at lower temperatures, we only performed such calculations at 353.15 K using long enough MD simulations.

All the molecular dynamic simulations were carried out using the parallel LAMMPS package.[80] The time step is set to 2 fs and the velocity−Verlet algorithm is used to integrate the equations of motion. The SHAKE algorithm is applied to all the bonds and angles related to hydrogen, with a tolerance of 10^{-4} and a maximum iteration of 10. The neighbor list is built with a skin distance of 0.2 nm every 5 steps. A cutoff of 1.2 nm is set for both the LJ and Columbic interactions. The LJ tail correction is added to the energy and pressure. The long-range electrostatic interactions are dealt with using the particle−particle particle mesh (PPPM) solver.

3. RESULTS AND DISCUSSION

3.1. Volumetric Properties. The liquid densities of neat [C_4mim][BF_4] and its water mixtures were simulated across the entire composition range at 1 bar and temperatures from 298.15 to 353.15 K. All the densities are given in Table 2. The

dx.doi.org/10.1021/jp3001543 | J. Phys. Chem. B 2012, 116, 3249−3263

Table 2. Simulated Densities for $[C_4mim][BF_4]$ (1)−H_2O (2) Mixtures at Temperatures from 298.15 to 353.15 K

mixture	simulated density (g/cm^3)					
	T = 298.15 K	T = 303.15 K	T = 313.15 K	T = 323.15 K	T = 333.15 K	T = 353.15 K
0	1.1994	1.1972	1.1888	1.1809	1.1732	1.1577
0.05	1.1992	1.1951	1.1864	1.1801	1.1727	1.1569
0.1	1.1981	1.1944	1.1857	1.1795	1.1710	1.1555
0.2	1.1962	1.1919	1.1838	1.1764	1.1686	1.1520
0.4	1.1883	1.1841	1.1760	1.1680	1.1603	1.1439
0.5	1.1837	1.1794	1.1705	1.1622	1.1543	1.1377
0.6	1.1761	1.1718	1.1631	1.1548	1.1467	1.1298
0.7	1.1650	1.1599	1.1524	1.1435	1.1348	1.1178
0.8	1.1441	1.1406	1.1322	1.1245	1.1152	1.0979
0.9	1.1069	1.1036	1.0953	1.0870	1.0786	1.0609
0.95	1.0692	1.0650	1.0584	1.0517	1.0421	1.0260
1.0	0.9938	0.9916	0.9873	0.9825	0.9760	0.9634

temperature dependence of densities of the neat $[C_4mim][BF_4]$ is given by a linear fitting

$$\rho_{IL,MD}/(kg\cdot m^{-3}) = 1430.2 \pm 4.14 - 0.771 \pm 0.013(T/K) \quad (2)$$

which coincides with the equation fitted from experiment[2]

$$\rho_{IL,expri}/(kg\cdot m^{-3}) = 1412.7 \pm 3.96 - 0.708 \pm 0.011(T/K) \quad (3)$$

The isobaric thermal expansion coefficient estimated through eq 2 is 6.43×10^{-4} K^{-1}, which is about 6% smaller than that by experiment, 6.89×10^{-4} K^{-1}.

Figure 2a shows a very good agreement between simulations and experimental data from different sources[72−74,81,82] at 298.15 K,

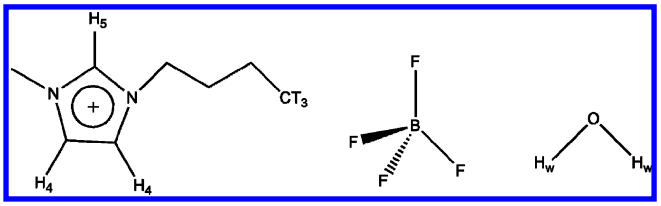

Figure 1. Chemical structures of 1-butyl-3-methylimidazolium tetrafluoroborate ($[C_4mim][BF_4]$) and water. The labeling of united atom CT3, ring hydrogen atoms H4, H5, and water hydrogen Hw is used in the text (section 3.5).

with absolute relative deviations (ARDs) within 0.5% over the entire composition range. A comparison of the simulation results and experimental data[72] from 303.15 to 353.15 K is given in Figure 2b. The ARDs slightly increase with the temperature, with the largest ARDs of about 1% at 353.15 K.

The excess molar volume, V_m^E, is difficult to obtain accurately by using both simulations and experiments. For $[C_4mim][BF_4]$/H_2O systems, it is about 3 order of magnitude less than the molar volume of neat $[C_4mim][BF_4]$. Thus, very small difference in density measurement can result in a large difference in excess molar volume. For example, the difference induced by 1% uncertainty in density is large enough to change the sign (positive or negative) of

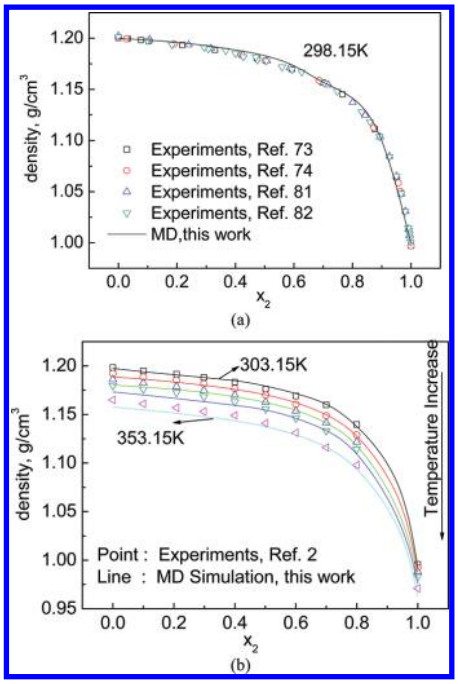

Figure 2. Simulated densities of $[C_4mim][BF_4]$ (1)−H_2O (2) mixtures as a function of water mole fraction x_2, compared with the experimental values at temperatures of (a) 298.15 K and (b) 303.15, 313.15, 323.15, 333.15, and 353.15 K.

the excess molar volume. As such, it is a much more stringent test of force field.[11,36] The excess molar volume is defined as

$$V^E{}_m = V_m - [x_1V_1 + x_2V_2] \quad (4)$$

where V_m, V_1, and V_2 are the molar volumes of the mixture, neat $[C_4mim][BF_4]$ and neat water, respectively. The quantity given in the square bracket is the molar volume of an ideal mixture.

In simulations, the uncertainty of V_m^E is only dependent on that of the box lengths L, which can be estimated by the block average method.[83] As given in Table 1 for simulations at 298.15 K, the relative uncertainty of L is typically 0.01% to 0.02%, leading to an uncertainty of V_m^E is 0.2 to 0.4 cm^3/mol in our simulations (Figure 3).

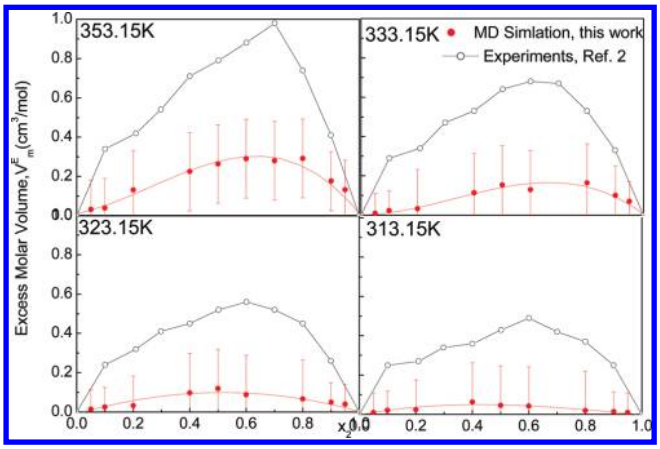

Figure 3. Excess molar volumes of $[C_4mim][BF_4]$ (1)−H_2O (2) mixtures predicted by molecular dynamics (MD) simulations, compared with experimental results at 313.15, 323.15, 333.15, and 353.15 K.

dx.doi.org/10.1021/jp3001543 | J. Phys. Chem. B 2012, 116, 3249−3263

As shown in Figure 3, the simulated excess molar volumes are positive, which is in agreement with experiment,[2,72] although the values are still less positive. It is an encouraging improvement against the previous negative values predicted by two widely used force fields.[53,54] The trend in experiments was also well reproduced that the excess molar volumes slightly increase with the temperature. We found that the reported excess volumes of IL/water mixtures by simulations are usually significantly more negative than their experimental values.[11,36,55] Kelkar et al.[36] proposed a reasonable explanation that water molecules experience a different polarized environment in the mixture and in neat water, in which the parameters of water are optimized. When they used a "least polarized" model for water, namely, with smaller oxygen charges, the simulation results are much better.

3.2. Excess Molar Enthalpy. The excess enthalpy is the change in enthalpy when mixing two neat liquids, which involves the disruption of interactions in the neat solvents and the establishment of interactions in the mixture. A rough interpretation of the excess enthalpy is the difference in the strength of interactions between unlike species and like species.[84] Thus, the excess molar enthalpy H_m^E is important for understanding the interactions between ions and water in IL/water mixtures.

The excess molar enthalpy, H_m^E, is computed as

$$H^E{}_m = H_m - [x_1H_1 + x_2H_2] \quad (5)$$

where H_m, H_1, and H_2 are the molar enthalpies of the mixture system, neat ionic liquid and water, respectively. The typical absolute uncertainty of H_m^E is about ±0.3 kJ/mol, as estimated by block average method,[83] the same as that done for V_m^E.

The simulated excess molar enthalpies of $[C_4mim][BF_4]$/H_2O mixtures for entire composition range are given in Table 4.

Table 3. Excess Molar Volumes, Self-Diffusion Coefficients, and Viscosities of $[C_4mim][BF_4]$ (1)−H_2O (2) Mixtures Calculated by Molecular Dynamics Simulations in This Work at 353.15 K

		$10^{10}D$, m^2 s^{-1}			
x_2	V^E_m, cm^3/mol	D_+	D_-	D_2	η, mPa·s
0.0	0	1.03	0.80	–	14.5
0.05	0.032	1.25	1.03	10.0	13.5
0.1	0.040	1.36	1.20	10.1	12.5
0.2	0.135	1.69	1.50	10.0	9.50
0.4	0.241	2.47	2.43	11.6	6.20
0.5	0.272	2.80	3.04	13.8	4.50
0.6	0.315	3.55	3.82	14.7	2.80
0.7	0.385	4.88	5.76	17.7	2.60
0.8	0.301	6.50	8.24	22.1	1.55
0.9	0.177	10.1	13.3	35.2	1.01
0.95	0.163	13.5	18.3	44.2	0.53
0.999	0.050	17.8	24.6	60.6	0.35
1.0	0	–	–	62.3	0.32

Very good agreement was found between the simulated and experimental values[2] at 298.15 K, as shown in Figure 4. The mixture presents endothermic behavior, indicated by the positive excess molar enthalpies. A slight increase of H_m^E with temperature was reported in experiments,[2] which is also well predicted by our simulations. For example, the maximum value of H_m^E increases from 2.106 kJ/mol at 298.15 K to 2.350 kJ/mol at 333.15 K

Table 4. Simulated excess molar enthalpies in of $[C_4mim][BF_4]$(1)-H_2O(2) mixtures at temperatures from 298.15 to 353.15 K

	excess molar enthalpies, kJ/mol					
x_2	T = 298.15 K	T = 303.15 K	T = 313.15 K	T = 323.15 K	T = 333.15 K	T = 353.15 K
0.05	0.296	0.326	0.350	0.378	0.416	0.687
0.1	0.700	0.711	0.769	0.825	0.911	0.941
0.2	1.259	1.305	1.451	1.500	1.521	1.554
0.4	1.979	2.180	2.243	2.340	2.357	2.465
0.5	2.224	2.301	2.400	2.483	2.502	2.600
0.6	2.163	2.232	2.284	2.440	2.461	2.547
0.7	1.992	2.072	2.158	2.200	2.360	2.454
0.8	1.562	1.718	1.811	1.840	1.871	2.048
0.9	0.888	1.051	1.091	1.141	1.167	1.285
0.95	0.496	0.511	0.559	0.600	0.730	0.860

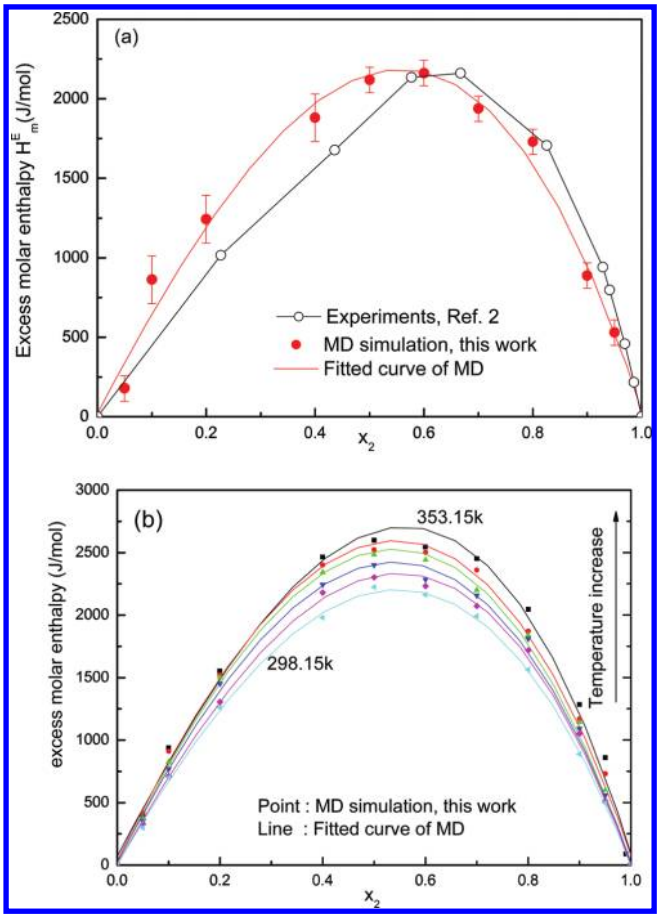

Figure 4. (a) Comparison of the experimental (hollow circles) and simulated excess molar enthalpy (solid circles) of $[C_4mim][BF_4]$ (1)−H_2O (2) mixtures, as a function of water mole fraction at 298.15 K. (b) Simulated excess molar enthalpies as a function of mole fraction of water at 298.15, 303.15, 313.15, 323.15, 333.15, and 353.15 K in this work.

measured by calorimeter,[2] which is 2.22 and 2.60 kJ/mol obtained by simulations.

3.3. Shear Viscosity. The shear viscosities at 353.15 K are calculated using Green-Kubo (GK) formula via equilibrium MD trajectories,

$$\eta = \frac{V}{10k_BT}\int_0^\infty \langle \sum_{\alpha\beta} P_{\alpha\beta}(0)P_{\alpha\beta}(t)\rangle \, dt \quad (6)$$

dx.doi.org/10.1021/jp3001543 | J. Phys. Chem. B 2012, 116, 3249−3263

where V is the volume of the system, T is temperature, and k_B is the Boltzmann constant. $P_{\alpha\beta}$ is the symmetrized traceless portion of the stress tensor $\sigma_{\alpha\beta}$, defined as

$$P_{\alpha\beta} = \frac{1}{2}(\sigma_{\alpha\beta} + \sigma_{\beta\alpha}) - \frac{1}{3}\delta_{\alpha\beta}\left(\sum_r \sigma_{\gamma\gamma}\right) \quad (7)$$

where $\delta_{\alpha\beta}$ is the Kronecker delta and $\delta_{\alpha\beta} = 1$ when $\alpha = \beta$, and otherwise $\delta_{\alpha\beta} = 0$. In this work, all nine components of the pressure tensor information are recorded at every time step and trajectories of 40 ns are used to calculate the viscosity. The details of the calculation method can be found in previous work.[67] Figure 5 shows the typical plateaus of the integrals of

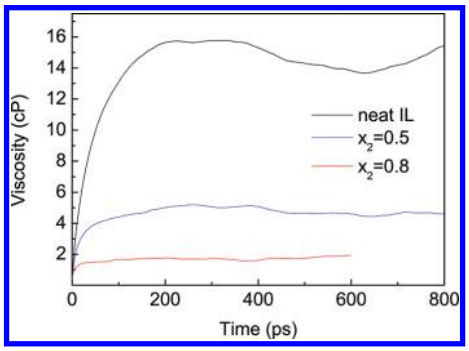

Figure 5. Viscosities of $[C_4mim][BF_4]$ (**1**)−H_2O (**2**) mixtures, estimated by the integral of correlation function via Green−Kubo formula using equilibrium molecular dynamics simulations.

the correlation functions. The uncertainty is estimated by the fluctuation. For example, the viscosity of neat $[C_4mim][BF_4]$ is estimated as 14.5 ± 1 cP in Figure 5.

As shown in Figure 6a, the simulated viscosities (Table 3) agree very well with those measured in experiments[72] in the water-rich region ($x_2 > 0.6$), while the values are systematically larger in IL-rich region. The viscosity of neat $[C_4mim][BF_4]$ (14.5 cP) is overestimated by our force field. To the best of our knowledge, the viscosities of the mixture of $[C_4mim][BF_4]$/water at 353 K were only reported in ref 72. However, their reported value for neat IL is 11.49 cP, about 10% smaller than those in recent measurements (13.3−14.1 cP).[75,85,86] Thus, it is more reasonable to compare the excess values of viscosity since we focus on the performance of the force field on mixing behavior in this work. Unlike the excess properties of volume/enthalpy, which are well-defined in classical thermodyamics, there are different models for viscosity of "ideal mixing". Here, we choose the logarithm model

$$\ln \eta^{id} = x_1 \ln \eta_1 + x_2 \ln \eta_2 \quad (8)$$

Where η_1 and η_2 are viscosities of neat IL and water, respectively. Thus, the nonideality of the mixture is characterized by[87]

$$\ln \eta^{E} = \ln \eta - (x_1 \ln \eta_1 + x_2 \ln \eta_2) \quad (9)$$

The calculated excess logarithm viscosities, η^E, were plotted in Figure 6b, coupled with the results measured by experiment.[72] The excess values are positive over the entire concentration range, in good agreement with experiments. The deviations in IL-rich region are still larger than those in water-rich region. As is discussed in section 3.1, the TIP4P-Ew model is optimized by the properties of neat water, reflecting the polarization effect of

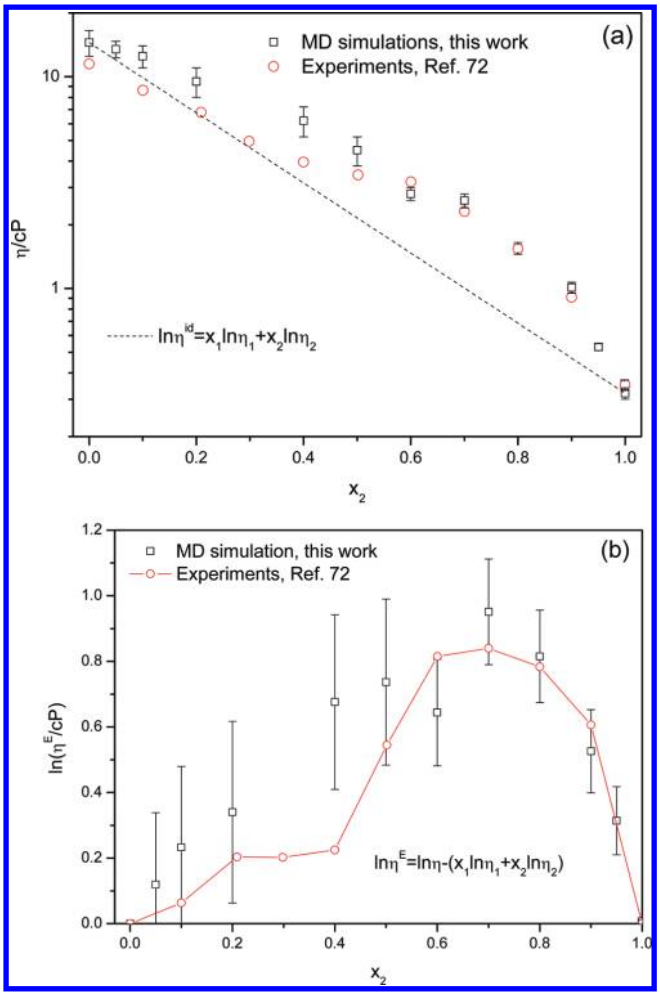

Figure 6. (a) Simulated viscosities (black squares) of $[C_4mim][BF_4]$ (**1**)−H_2O (**2**) mixtures at 353.15 K, compared with experimental values (red circles). The dashed line represents ideal mixing. (b) Same as part a, while excess logarithmic values of viscosity are compared.

water molecule. However, the local environment of water molecules is significantly different in IL as they are in neat water, which is confirmed by various properties discussed below. Therefore, it is expected to get better results by using polarized force fields, or alternatively, by empirical non-LB combination rules. However, it is beyond the purpose of this work.

3.4. Self-Diffusivity. The self-diffusion coefficients of the ions and water molecules at 353.15k are calculated from the MD trajectories using the Einstein relation

$$D_i = \frac{1}{6}\lim_{t\to\infty}\frac{d}{dt}\langle[\vec{r}_i(t) - \vec{r}_i(0)]^2\rangle = \frac{1}{6}\lim_{t\to\infty}\frac{d\Delta r_i^2}{dt} \quad (10)$$

where the quantity in ⟨...⟩ is the mean-square displacement (MSD) of species i. Because of the high viscosity and overall "sluggishness" of ILs, it is necessary to carry out relatively long MD runs in order to reach the true diffusive regime so that the estimated values are in a reliable accuracy.[88] In this work, we use MD trajectories as long as 40 ns to calculate the MSD, by which the diffusion coefficients were estimated using the linear fitting to the 4−10 ns slope. A typical plot of MSD is shown in Figure 7a for neat $[C_4mim][BF_4]$ at 353.15 K. The simulated self-diffusion coefficients are 1.03 × 10^{-10} m^2 s^{-1} for cations

dx.doi.org/10.1021/jp3001543 | J. Phys. Chem. B 2012, 116, 3249−3263

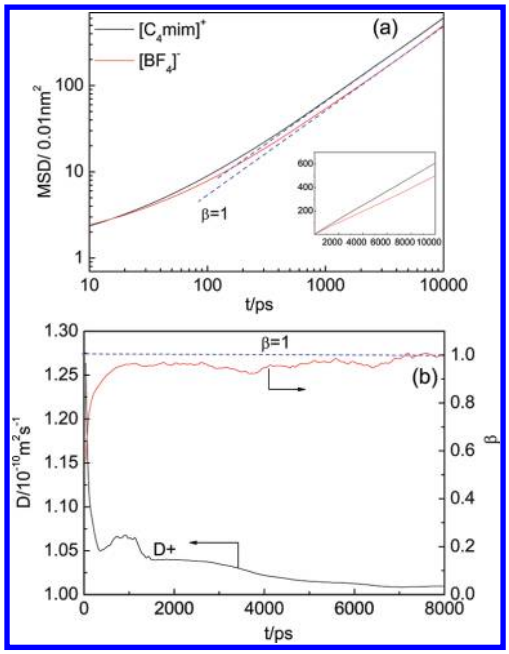

Figure 7. (a) Mean square displacements (MSDs) of cations and anions in neat $[C_4mim][BF_4]$ in log−log scale at 353.15 K, calculated using 40 ns molecular dynamics trajectories. The diffusion limit of slope of 1 ($\beta = 1$) is shown as blue dashed line. A linear−linear scale plot is shown in inset figure. (b) Self-diffusion coefficients of cation in neat $[C_4mim][BF_4]$ at 353.15 K, by fitting slopes of MSD at different time spans from part a. The value of $\beta(t) = (d(\log \Delta r_i^2(t))/d(\log(t))$ is shown as a red line.

and 0.80×10^{-10} m^2 s^{-1} for anions, which coincide well with our previous reported values.[62] They are also in good agreement with the experimental values of 1.00×10^{-10} m^2 s^{-1} and 0.84×10^{-10} m^2 s^{-1}, measured by NMR method.[75]

In general, the self-diffusion coefficients for both ions and water molecules increase when water is added to IL, as shown in Figure 8. An exponential dependence of the self-diffusion coefficients can be well obtained by linear fitting between ln D and x_2 ($\ln D = A + Bx_2$). For water diffusion, three distinct regions are clearly reflected by different values of B with the increase of water concentration. When small amount of water is added into IL ($x_2 < 0.2$), the self-diffusion coefficients are nearly the same, indicating water molecules experience a very similar environment. It is reasonable because a stable polar network is formed in IL due to the strong interaction between cations and anions, which is less disturbed by adding small molecules such as water. The diffusion of water is somehow similar to that in solid framework such as zeolite, although there are no "pores" (cavities) larger enough to accommodate a water molecule. Instead, the ions adjust slightly their relative position/orientation[89] when water is inserted. When more water is added ($0.2 < x_2 < 0.8$), water molecules tend to aggregate to clusters, such as dimer, trimer or more (see section 3.5 for quantitative results by simulation). As the result, the cation−anion network is also weakened and weakened correspondingly. When there are enough water molecules ($x_2 > 0.8$), they would percolate the whole space and the system is transformed from IL-rich to water-rich mixture.

The diffusion of ions also exhibits similar evolvement (Figure 8c), although not as significant as that of water. It is interesting to note the different behaviors of cations and anions. Generally, the effect of water on the diffusion of anion is more significant than that of cations (with larger B values). It maybe indicates stronger interactions between the anion and water. A clear turnover of relative mobility between cations and anions is observed at around $x_2 = 0.4$ in simulations. In neat $[C_4mim][BF_4]$, the cation, although larger than anion, diffuses slightly more quickly, which is verified by using both experiments[75] and simulations.[44] When water is added, the difference becomes smaller and smaller. Eventually, the anions exhibit faster dynamics in mixtures when water mole fraction is beyond 0.4. Similar results were also reported in simulations of the dilute aqueous $[C_6mim][PF_6]$ by Raju and Balasubramanian.[44]

To the best of our knowledge, no experimental values of self-diffusion coefficients were reported for $[C_4mim][BF_4]$/water mixtures.

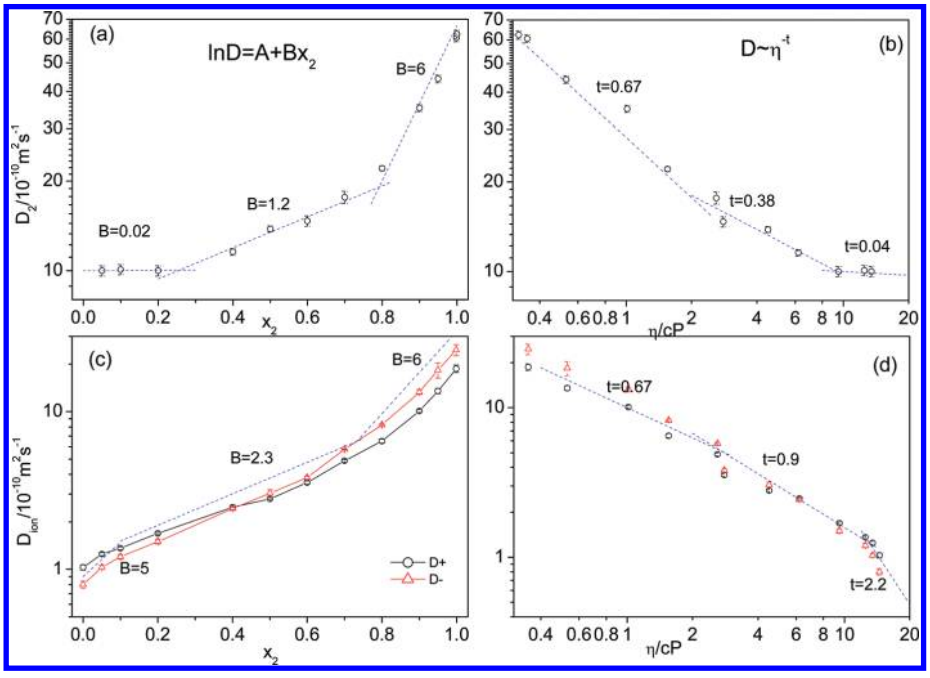

Figure 8. Simulated self-diffusion coefficients of water (a) and ions (c) in $[C_4mim][BF_4]$ (**1**)−H_2O (**2**) mixtures at 353.15 K as a function of mole fraction of water. The relationship between self-diffusion and viscosity at different water concentrations is shown in log−log scale for water (b) and ions (d).

dx.doi.org/10.1021/jp3001543 | J. Phys. Chem. B 2012, 116, 3249−3263

However, the mutual diffusion coefficients of ILs were measured by Taylor dispersion technique at infinite dilute concentration in water.[90−92] The diffusion coefficient of $[C_4mim][BF_4]$ in water, D_{12}, is 26×10^{-10} m^2 s^{-1} at 353 K, as extrapolated by experimental data. In our simulation, D_{12} can be estimated via the Nernst−Hartley equation:[50]

$$D_{12} = \frac{2D_+D_-}{D_+ + D_-} \tag{11}$$

Here D_+ and D_- are the self-diffusion coefficients of the cations and anions in water at infinite dilution (without any association), respectively. The simulated D_+ and D_- at infinite dilution (x_2 = 0.999) are 17.8×10^{-10} m^2 s^{-1} and 24.6×10^{-10} m^2 s^{-1}, respectively. Thus, D_{12} is estimated as 20.6×10^{-10} m^2 s^{-1}, which is slightly smaller than the experimental value.

The diffusion of molecules is highly correlated to the viscosity of the fluids. The classical Stokes−Einstein (SE) relation is often used:

$$D = \frac{kT}{c\pi\eta r_{\text{eff}}} \tag{12}$$

where r_{eff} is the effective hydrodynamic radius, k is the Boltzmann constant, T is temperature, and c is a dimensionless parameter ranging from 4 (slip) to 6 (stick) dependent on the boundary conditions. Here, the effective hydrodynamic radius is calculated by choosing c as 6, as shown in Figure 9. The

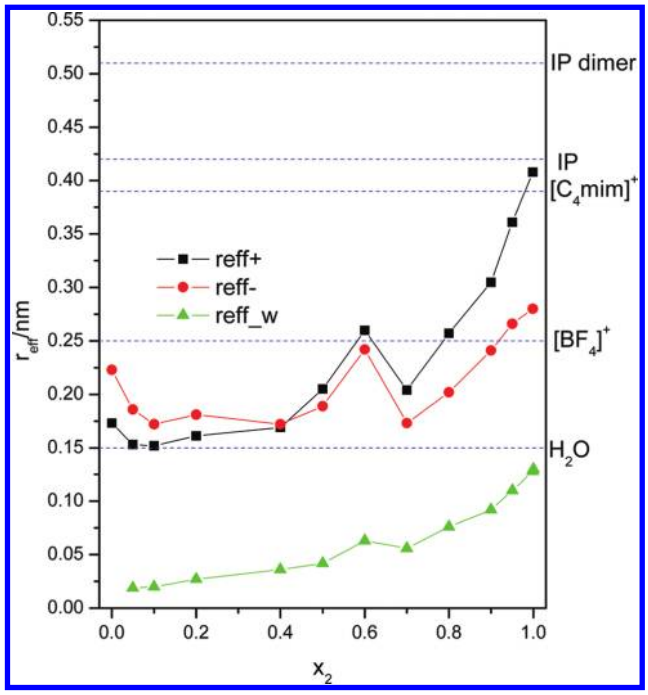

Figure 9. Effective hydrodynamic radius calculated by the classical Stokes−Einstein (SE) relation from simulated values of self-diffusion coefficients and viscosities in $[C_4mim][BF_4](1)$-$H_2O(2)$ mixtures, for (■) cation, (red ●) anion and (green ▲) water. The dotted lines represent the values of van der Waals (vdW) radii for different species calculated from vdW volumes at B3LYP/6-31+G* level.

values of van der Waals (vdW) radii for different species in the mixture are also shown for comparison, which are calculated from vdW volumes at B3LYP/6-31+G*. Clearly, the effective hydrodynamic radii are significantly smaller than their vdW radii, by about a factor of 2 in the IL-rich region. The results are consistent with those reported for other neat ILs and their binary mixtures.[93,94] Koddermann and Ludwig[93] investigated the mixture of $[C_2mim][Tf_2N]$/chloroform in detail by MD simulations. They found the too small r_{eff} obtained from eq 12 can be related to dynamical heterogeneities in the solutions. At the very low IL concentration, they found that the SE relation leads to quite reasonable effective radii, in which no dynamical heterogeneity is detected. As can be seen in Figure 9, the effective radii approach their vdW radii very well when diluting the IL in water. This is different from the system of $[C_2mim][Tf_2N]$/chloroform at low IL concentration, in which large IL clusters and collective diffusion are found. In our simulations, the aggregation between cations and anions is indicated by the followed analysis of microscopic structure (section 3.5) at water mole fractions around 0.9. However, it is not strong enough to make the cations and anions diffuse collectively.

A fractional Stokes−Einstein relation ($D \sim (T/\eta)^t$) was found valid for neat ILs, where $0.5 < t < 0.95$.[94] Here, we analyze the relation by the log D−log η plot in Figure 8, parts b and d. Consistent with the $D \sim x_2$ relation, the three distinct regions are also reflected in the figures. It is noteworthy that a same t value of 0.67 is obtained for both the water and ion diffusion in the water-rich region. While in other case the t value for water is much smaller than that for ions, indicating there is significant local heterogeneity in the concentration range of $x_2 < 0.8$. In the IL-rich region ($x_2 < 0.2$), the t values are 0.04 and 2.2 for water and ions, respectively. These "abnormal" values reflect the very different behavior when small amount of water is adding into IL, compared with those in common fluids.

3.5. Local Structure and Water Clustering. The radial distribution function (RDF) represents the spherically averaged local organization around a center site or atom, giving the probability of finding another particle in the distance r. It is one of the important tools to characterize the local structure of dense fluids, reflecting the effective pairwise interaction, i.e., the potential of mean force, between two species. The local environment around a site or atom j can be properly represented by the coordination number, $N_{ij}(r)$, which is the average number of the site or atom i within a sphere of radius r_c around j, calculated by the integral of RDF.

The cut off radius r_c is usually chosen to be the first local minimum of corresponding RDF, which represents the first solvation shell. In contrast to the spherically averaged RDF, the orientational local structure, i.e., three-dimensional distribution of an atom around a given molecule can be depicted by the space distribution function (SDF), which is well visualized by gOpenMol. In this work, to demonstrate the structural evolution in the mixtures, we plot the SDF contours in the same absolute density, instead of the usually used relative values.

The heterogeneity of the local structure is often caused by forming clusters in different size. In this work, water clustering is analyzed by the connectivity of water−water pairs. Two water molecules are considered to be "connected" by a simplified geometric criterion, i.e., the O−O distance is less than 0.35 nm, corresponding to the approximate minimum of the O−O RDF. The connectivity of water is stored in a $N \times N$ matrix, where N is the number of water molecules in the simulation box. If there is not any connectivity of a water molecule with all other water molecules, it is a water monomer, or "isolated" water. If two water molecules are connected while without any connectivity of other water molecules, the water dimer is formed. Larger

dx.doi.org/10.1021/jp3001543 | J. Phys. Chem. B 2012, 116, 3249−3263

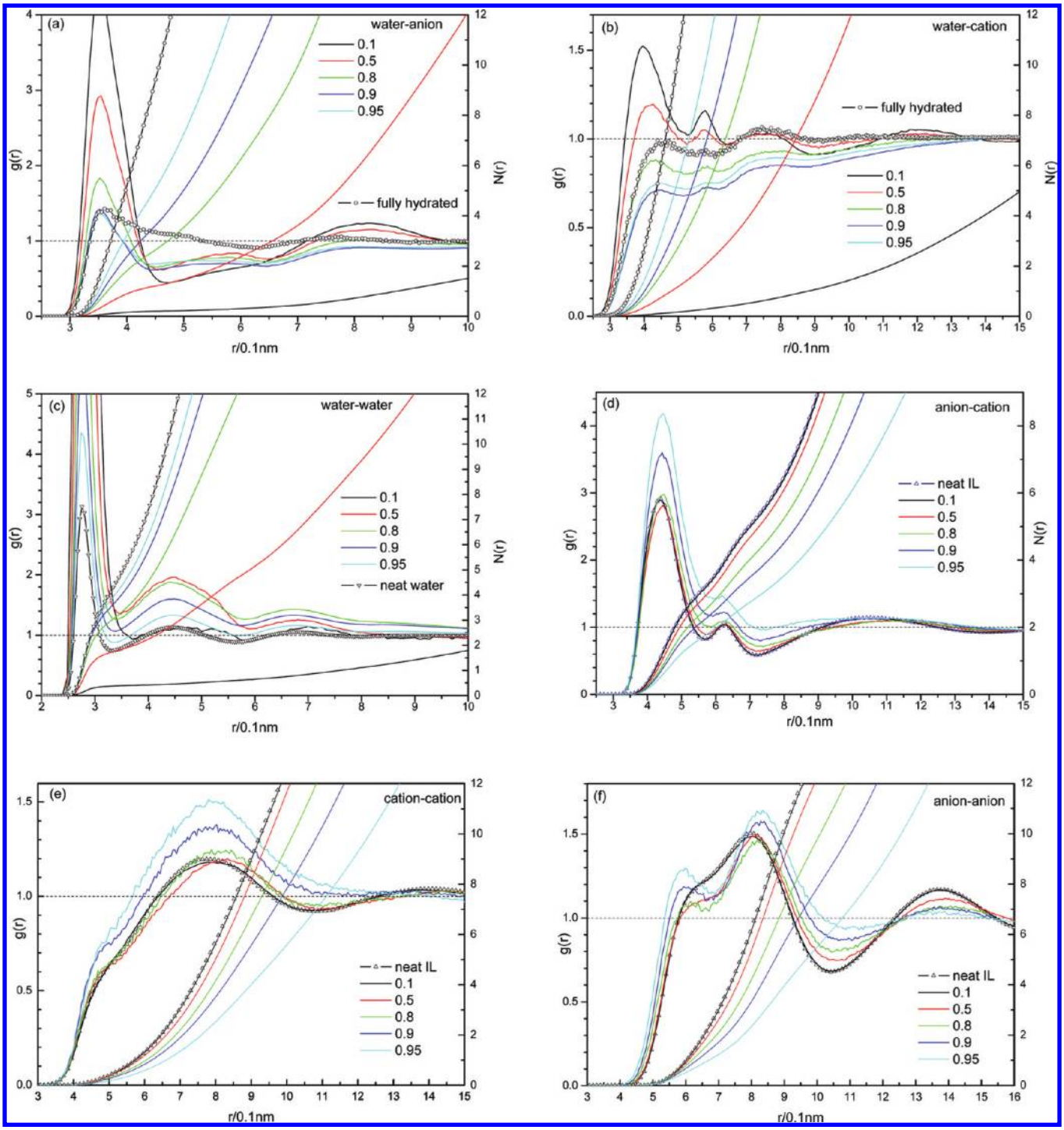

Figure 10. Center of mass (COM) based radial distribution functions (RDFs) and coordination number integrals among the cation ($[C_4mim]^+$), anion ($[BF_4]^-$) and water in $[C_4mim][BF_4]$ (**1**)−H_2O (**2**) mixtures. (a) water−anion; (b) water−cation; (c) water−water; (d) anion−cation; (e) cation−cation; (f) anion−anion.

clusters such as trimer, tetramer, etc., can be also discriminated similarly by further analysis. Thus, the distribution of the water cluster size is obtained by ensemble average. The connectivity matrix can also be used to analyze the nearest-neighbors of a center water molecule, by which the local environment around water is obtained in more detail than the averaged coordination number.

The center of mass (COM) based RDFs are depicted for anion−water, cation−water, water−water, cation−anion, cation−cation, and anion−anion in Figures 10, accompanied by the corresponding coordination number integrals. In the studied concentration range, the positions of first peak for all these RDFs do not show any detectable shift in our simulations except that of cation−water RDF (see below). The same thing is found for the site−site RDFs, indicating the structure in the first solvation shell is determined mainly by the short-range interaction (LJ term in eq 1). In contrast, the peak values are strongly dependent on the amount of water, which is controlled by the relative intensity of the interactions between different species in the mixture. Therefore, we extract the first peak

dx.doi.org/10.1021/jp3001543 | J. Phys. Chem. B 2012, 116, 3249−3263

values to detect their response to the adding of water, as shown in Figure 11.

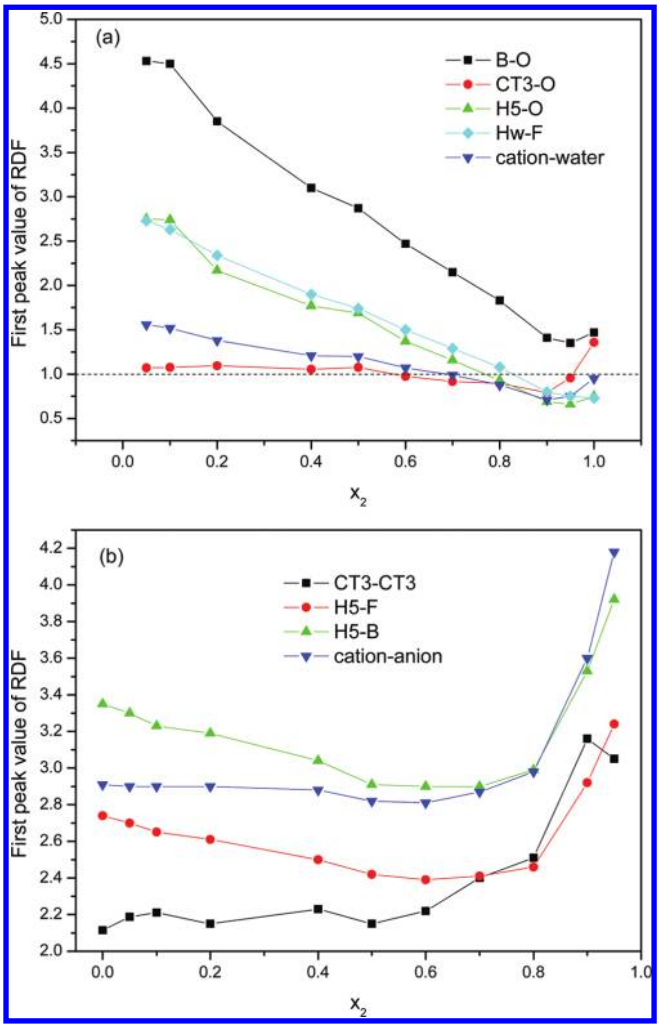

Figure 11. First peak value of the site−site radial distribution function (RDF) as a function of water mole fraction (x_2) in $[C_4mim][BF_4]$ (**1**)−H_2O (**2**) mixtures. For atom notations, see Figure 1.

Water−Anion Interation. It is clear that the correlation between anion and water is more significant than that of cation and water, in accordance with the results by Schröder et al.[33] that the water-cation network can not be well established in the mixture. The first peak value at 0.35 nm in water−anion RDF continues to decrease from 4.53 to 1.35 as the water mole fraction increases from 0.05 to 0.95 (Figures 10a and 11a). A "turnover" can be inferred by the RDF in full hydration (infinite dilute aqueous IL solution), not only by a small increase of the peak value, but also by the blurring of the first solvation shell (Figure 10a). In fact, the low possibility to find water around $[BF_4]^-$ at the range of 0.45−0.65 nm is caused by the strong interaction between the cations and anions (see the discussion below). The wide second peak at 0.82 nm reflects the correlation between anion and water distributed in the different region around a cation (Figure 12), which is weakened at higher water amount and disappears at infinite dilute solution. As demonstrated by the three-dimensional SDFs in Figures 13, the preferable positions of water are above the middle of the six edges formed by four B atoms, and then, on the top of the four triangles of the tetrahedral $[BF_4]^-$.

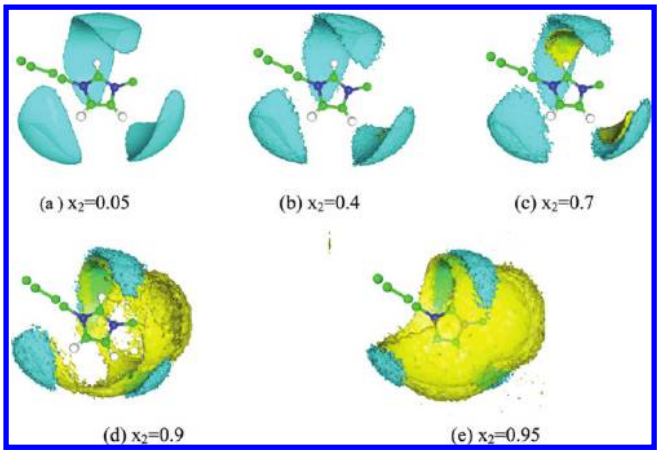

Figure 12. Three-dimensional probability distributions of O in water (yellow) and B in $[BF_4]^-$ anion (cyan) around $[C_4mim]^+$ cation at various concentrations in $[C_4mim][BF_4]$ (**1**)−H_2O (**2**) mixtures. The contours are drawn in the same absolute densities of 45 mol/L (27/nm^3) for O and 30 mol/L (18/nm^3) for B.

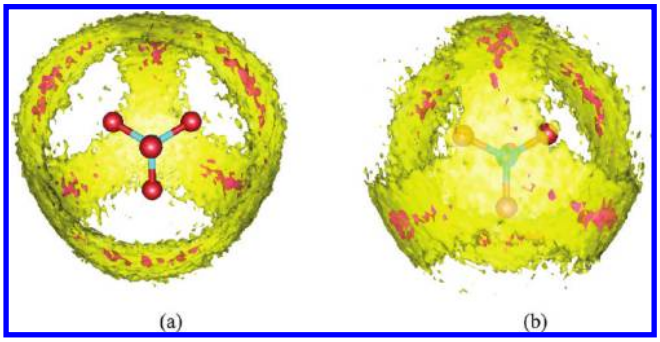

Figure 13. (a) Three-dimensional probability distributions of O in water around $[BF_4]^-$ anion at x_2 = 0.9 in $[C_4mim][BF_4]$(1)-H_2O(2) mixture. The colors indicate the contour levels of 3.5 (red) and 2.0 (yellow), corresponding with the absolute water densities of 90 and 51 mol/L (54/nm^3 and 31/nm^3), respectively. (b) Same as part a in another perspective view.

Water-cation interaction. At lower water concentration, it is observed three weak but distinct peaks in the first solvation shell (Figure 10b), reflecting the asymmetry of the cation. The position of the first peak is shifted about 0.05 nm with the increase of water amount, i.e., from 0.39 nm at x_2 = 0.05 to 0.44 nm at x_2 = 0.95. The second and third peaks locate at 0.58 and 0.75 nm, respectively. In combination of Figure 12, we found the first two peaks represent the three distributions around the imidazolium ring, since the COM of the cation is off the ring center and near the butyl side. The third peak reflects distribution around the butyl group. As the water is added, the first peak value decreases from 1.6 at x_2 = 0.05 and is less than unity when x_2 > 0.7, then, reaches a minimum of 0.7 at x_2 = 0.9, where a "turnover" responsible to the aggregation of IL (see below) is observed. By comparing the first peak values of H_5-O, CT_3-O and cation−water RDFs in Figure 11a, we found that the turnover is contributed mostly by the rapid increase of the correlation between CT_3 and water when x_2 > 0.90, since the minimum of H_5-O is at x_2 = 0.95, the same value for B−O RDF. In the case of full hydration, the peak at 0.75 nm is more significant than the first two at 0.44 and 0.58 nm (Figure 10b), indicating hydrophobic solvation dominates in the state. More interestingly, the water concentration dependence of the first

dx.doi.org/10.1021/jp3001543 | J. Phys. Chem. B 2012, 116, 3249−3263

peak values of Hw-F and H_5-O RDFs are nearly the same (Figure 11a). Therefore, the asymmetry and larger size of the cation should be responsible to the weaker interaction between cation and water, since the anion $[BF_4]^-$ is near-spherical.

Ionic Liquid Aggregation. As indicated by the RDFs between the cation and anion (Figure10d–f), the IL structure (polar network) maintains very well until the water mole fraction reaches 0.8. It is not surprising since water is much smaller than both cations and anions, and the weight percent of water at x_2 = 0.8 is around 25%. As x_2 increases to 0.8, about 7 water molecules intrude into the first solvation shell of the cation, while the number of neighbored anion around the cation decrease about 1. This is achieved by slight rearrangement of the anion distributions, as shown by a drop of the anion–anion RDF in the range of 0.55 to 0.75 nm (Figure 10f). A subtle change in anion–anion RDF is also observed at x_2 = 0.8, i.e., a small peak appears within 0.5 to 0.6 nm, which is a signal of water separated anions. As water is added after x_2 > 0.8, the signal is further enhanced. In addition, the whole RDFs of cation–anion, cation–cation and anion–anion are up-shifted continuously with the increase of water, and nearly all the values are larger than unity within 1.3 nm when x_2 = 0.95, indicating the aggregation of IL occurs in the solution. Accordingly, the RDFs of cation-water are down-shifted, reach a minimum at x_2 = 0.9, and increase again afterward. This means the rearrangement is not sufficient to accommodate more and more water molecules after x_2 = 0.8. Therefore, the mixture is switched from IL-rich (water in IL) to water-rich (IL in water) region. The evolution is demonstrated more intuitively by the SDFs in Figure 12.

The aggregation of $[C_4mim][BF_4]$ in aqueous solution was reported by many experimental studies. Singh and Kumar[6] summarized the critical aggregation concentrations (CACs) deduced using various methods, which range from IL concentrations 0.7 to 0.95 mol/L (about x_2 = 0.98). Bowers et al.[4] inferred from SANS data that the aggregation occurs at the IL concentrations of 0.8 to 3.0 mol/L (about x_2 = 0.98 to 0.88), and the maximum exists at 2.0 mol/L (about x_2 = 0.945). Almasy et al.[5] found the strongest inhomogeneity exists at x_2 = 0.93 by concentration fluctuation and Kirkwood-Buff integral calculations from SANS data, which is in accordance with the phase segregation concentration at the upper critical solution temperature (USCT) of 277 K.[2] Jeon et al.[25] also reported the mixture structure appears qualitative changes at water concentrations of 32 and 45 mol/L (x_2 = 0.93 and 0.98) evidenced by IR and Raman spectral features. The simulations here show that the aggregation is evidenced when x_2 > 0.8 and reaches maximum at the water mole fraction between 0.9 and 0.95 (Figure 10b), which coincides well with these studies.

It is well-known that the imidazolium has amphiphilic surfactant-like structure with two different parts: the hydrophilic "head" (ring, represented by H_5) and the hydrophobic "tail" (alkyl chain, represented by CT_3). Taking a look at the concentration dependent first peak values of site–site RDFs between cations and anions (Figure 11b), we found the intruding water slightly weaken the correlation of head-anion, while has little effect on that of tail–tail when x_2 < 0.6. The tail–tail correlation is enhanced by water when x_2 > 0.6, much earlier than 0.8 for head-anion. However, no evidence of the significant tail–tail aggregation is observed in simulations. As shown in Figure S2, Supporting Information, both the tail–tail and head–anion complexes can be found in the snapshot at x_2 = 0.95. Thus, the aggregation in aqueous $[C_4mim][BF_4]$ is a result of the collaboration of the strong electrostatic attraction between counterions and the accumulation between hydrophobic tails. Recent simulations showed the latter will become a dominant factor when the tail is as long as octyl.[40,52] The IL aggregation is closely dependent on the nature of anion and cation. For example, Bernardes et al. showed that[56] the aggregation of $[C_2mim][EtSO_4]$ in water occurs without any evidence of tail–tail accumulation when x_2 > 0.95 by simulations.

Water Clustering. The sharp and high peaks in Figure 10c indicate the water molecules tend to aggregate in $[C_4mim][BF_4]$. Further cluster analysis is carried out by the method described in the beginning of section 3.5. Figure 14 shows the

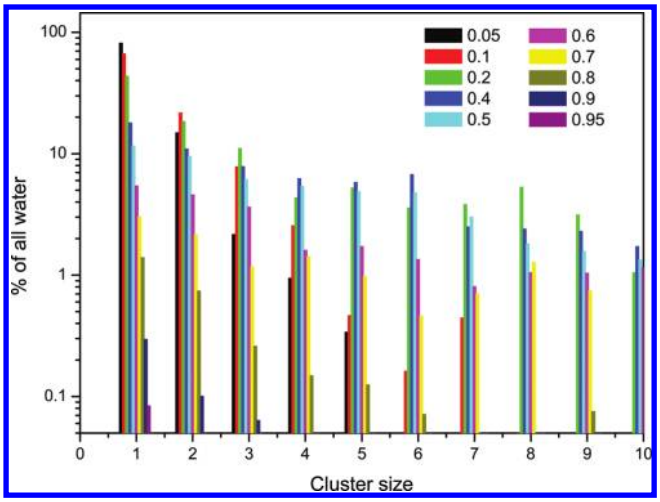

Figure 14. Size distributions of water cluster (smaller than 10-mer) at various water mole fractions in $[C_4mim][BF_4]$ (**1**)–H_2O (**2**) mixtures. The vertical coordinate represents the percentage of water molecules to form the corresponding cluster.

percentage of water which forms a cluster smaller than 10-mer at various concentrations. The percentage of the monomer ("free" water which does not connect with any other water molecules) decrease exponentially from 82% at x_2 = 0.05 to 0.08% at x_2 = 0.95. It is noteworthy that the distribution of small clusters nearly disappears (<1%) when x_2 > 0.8. The full spectrum of cluster distribution and the number of water neighbors around a center water molecule are shown in Figures 15 and 16, respectively. The corresponding snapshots are given in Figures S1.

The molecular state of water in ILs can be experimentally detected by NMR, IR and Raman spectroscopies. As regards to water in $[C_4mim][BF_4]$, Cammarata et al.[14] found that only one molecular state exists at lower water concentration (up to $x_2 \sim 0.12$), in which water is bounded simultaneous to two anions, as indicated by the two vibrational modes observed at 3560 and 3640 cm^{-1}. Masaki et al.[24] observed other two broad bands at 3250 and 3450 cm^{-1} appear when x_2 > 0.06, indicating the formation of water clusters. Lendl et al. also detected a second type water state when x_2 > 0.04 with the help of multivariate curve resolution technique,[18] which is consistent with the observations of far-infrared spectra in the range from 600 to 20 cm^{-1}.[19] In our simulations, significant amount of dimer exist when x_2 < 0.2. For example, 15% and 21% of the water molecules are found in dimer at water mole fractions of 0.05 and 0.1, which contributes to a different vibrational mode from the water monomer bounded by two anions. Figure 17 demonstrates the typical configurations of "free" water and water dimer in the solution. In our simulations, we found that

dx.doi.org/10.1021/jp3001543 | J. Phys. Chem. B 2012, 116, 3249–3263

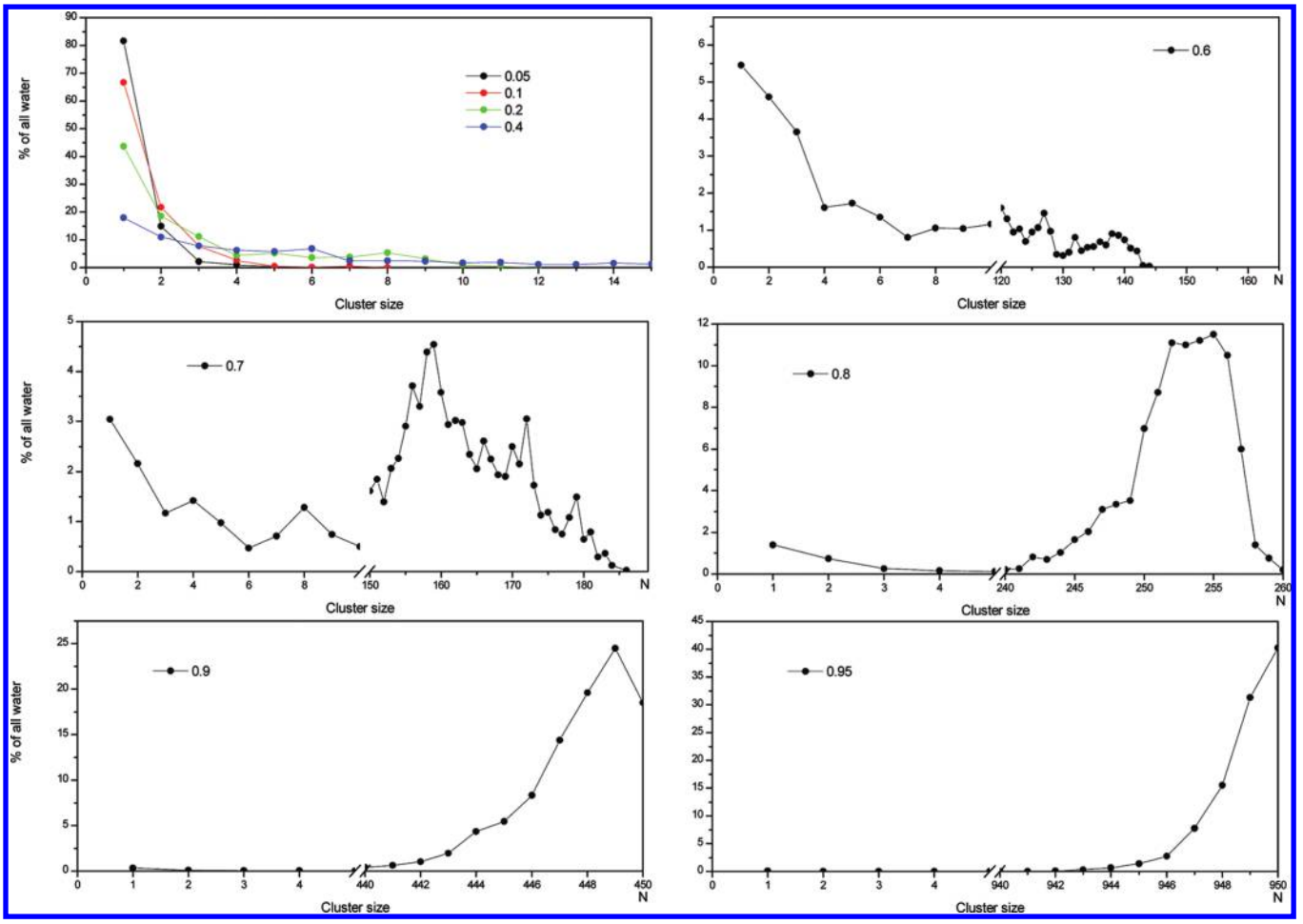

Figure 15. Size distributions of water cluster at various water mole fractions in $[C_4mim][BF_4]$ (**1**)−H_2O (**2**) mixtures. *N* represents the total number of water molecules in the simulation box (see Table 1 for details).

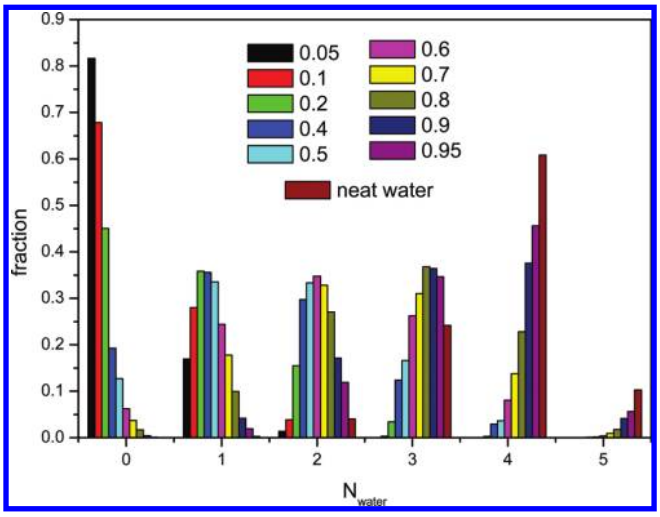

Figure 16. Distribution of the number of neighbored water molecules (N_{water}) around a center water molecule.

the water monomer formed two hydrogen bonds with two anions is usually also the nearest neighbor of two cations, via hydrogen bonds between O and either H_5 and H_4, as shown in Figure 17a. In fact, the coordination numbers of anion and cation around a water molecule are both close to 2 when x_2 < 0.1, although the latter value is slightly smaller due to the steric hindrance of alkyl chains in the cations. The result is not strange since the concentration dependent first peak values of Hw-F and H_5−O are very similar (Figure 11a). It is also consistent with the observations in NMR studies.[8]

Only small clusters can be found in the mixture when small amount of water is added. For example, more than 99% of the clusters are smaller than 10-mer at x_2 = 0.2. Both the size of cluster and the percentage of larger clusters increase rapidly with the water concentration. Large water clusters appear to dominate the distribution when x_2 > 0.7. As shown in Figure 15, most of the cluster size is near the limit of simulation box at x_2 = 0.8, indicating a single large water cluster forms in the mixture, i.e., the percolation of water. As discussed in above sections, the system transforms from IL-rich to water-rich mixture after this concentration. It is interesting that the threshold value of x_2 = 0.8 was also found for $[C_2mim][EtSO_4]$/water mixture by recent simulations,[56] at which the volume fraction of water is 0.25, the same as that of $[C_4mim][BF_4]$/water. It seems that the concentration of water percolation is determined by the volume fraction and weakly dependent on the nature of ions, since $[EtSO_4]^-$ is more hydrophilic anion.

In summary, the two "turnover" points of x_2 = 0.2 and 0.8, as reflected in the concentration dependent viscosities and self-diffusion coefficients (Figure 8), are well related to the local structural evolution discussed in this section. At the water mole fraction below 0.2, most of the water molecules are isolated in the polar network constituted by cations and anions. Therefore,

dx.doi.org/10.1021/jp3001543 | J. Phys. Chem. B 2012, 116, 3249−3263

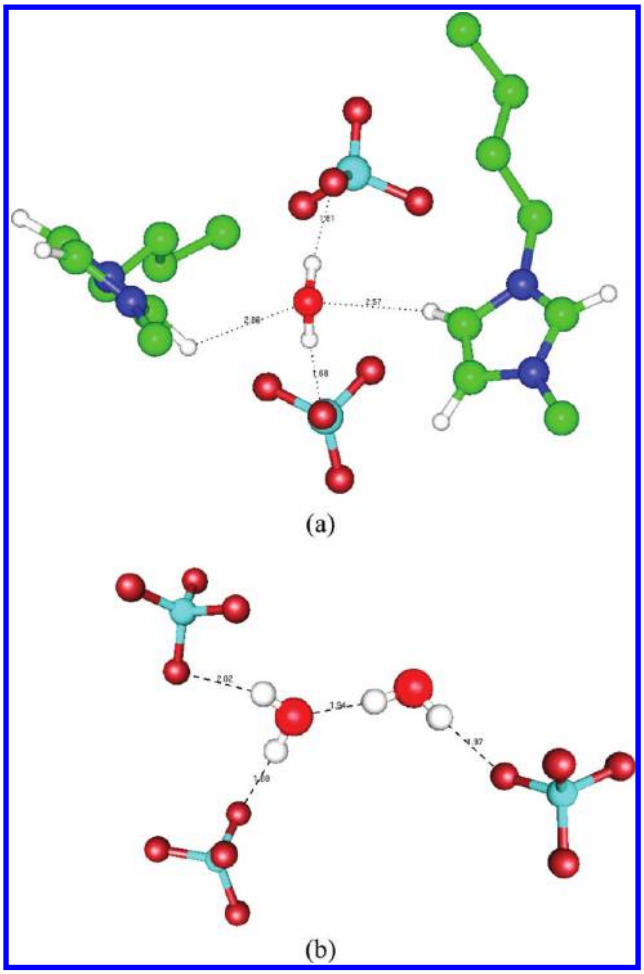

Figure 17. Typical molecular complexes between water and cation/anion in $[C_4mim][BF_4]$/water mixture at water mole fraction of 0.1.

the diffusion of water is weakly dependent on the concentration. As more water is added, they tend to form larger clusters and weaken the cation−anion interactions. The IL network is slightly adjusted to accommodate the added water molecules until x_2 = 0.8, at which water molecules percolate the whole system and about one anion is expelled from the first solvation shell of the cation. After this concentration, IL starts to dissolve in water, though not in the form of isolated cations and anions, but in small clusters by the aggregation of cations and anions.

4. CONCLUSIONS

Despite lots of simulations on ionic liquids/water mixture, relative few studies focus on the quantitative comparisons between simulated and experimental properties covered the entire concentration range. Extensive molecular dynamics simulations for $[C_4mim][BF_4]$/water mixtures are performed using our recently proposed united-atom force field combined with TIP4P−Ew water model. Cross parameters are obtained by the Lorentz−Berthelot (LB) combining rules without further optimization. The simulated densities, excess molar volumes, excess molar enthalpies, self-diffusion coefficients and viscosities are compared with available experimental data. In addition, the local structure, as characterized by radial distribution functions (RDFs), spatial distribution functions (SDFs) and water clustering analysis, is used to elucidate the connection between structure evolution and the macroscopic observations in simulations.

The absolute relative deviations of liquid densities are within 0.5% over entire concentration range at 298.15 K and slightly increase to about 1% at 353.15 K. The positive excess molar volume and excess molar enthalpy, as well as their dependence on temperature, are well reproduced in our simulations. The simulated viscosities are also in good agreement with experimental values, especially in the water-rich region. The self-diffusion coefficients, D_i, show an exponential dependence on the mole fraction of water x_2. The diffusion of cation is less affected by the adding of water. Thus, the anion is found to diffuse faster than the cation when $x_2 > 0.4$, in contrast to the results in neat IL. Three distinct regions are reflected from the B values by fitting $\ln D_i = A + Bx_2$. At low water concentrations of $x_2 < 0.2$, most of water molecules are isolated each other and experience a local environment in the polar network nearly the same as that in neat IL. In the concentration range of x_2 = 0.2 to 0.8, water molecules tend to form clusters by self-aggregation. The size of clusters increases with the mole fraction of water, slightly disturbing the polar network of IL. When there are enough water molecules, small clusters are all connected with each other to form a single large cluster. Thus, the IL is percolated by water molecules at x_2 = 0.8. The mixture is transformed from IL-rich region to water-rich region. In the water-rich region, our simulation evidenced a moderate degree of IL aggregation, due to a hybrid effect of the strong electrostatic attraction between caions and anions, and the accumulation of hydrophobic tails in cations. The maximum degree of aggregation appears in the concentration range of x_2 = 0.9 to 0.95.

■ ASSOCIATED CONTENT

Supporting Information

All force field parameters are given in Table S1, densities by simulations of different box sizes are given in Table S2, Figure S1 provided the comparisons of the center-of-mass radial distribution function of water and anion calculated in different size simulations, and Figure S2 showed the snapshots in mixtures of x_2 = 0.05, 0.1, 0.2, 0.4, 0.5, 0.6, 0.7, 0.8, 0.9, and 0.95. This material is available free of charge via the Internet at http://pubs.acs.org

■ AUTHOR INFORMATION

Corresponding Author

*E-mail: (Z.L.) liuzhp@mail.buct.edu.cn; (D.C.) caodp@mail.buct.edu.cn.

Notes

The authors declare no competing financial interest.

■ ACKNOWLEDGMENTS

Financial support of the Natural Science Foundation in China (Nos. 20976004 and 21176009) is gratefully acknowledged. We also thank the computational resources provided by Supercomputing Center of China Academy of Sciences (SCCAS) and Chemical Engineering Grid Computing Center in Beijing University of Chemical Technology

■ REFERENCES

(1) Plechkova, N. V.; Seddon, K. R. *Chem. Soc. Rev.* **2008**, *37*, 123−150.

(2) Rebelo, L. P. N.; Najdanovic-Visak, V.; Visak, Z. P.; da Ponte, M. N.; Szydlowski, J.; Cerdeirina, C. A.; Troncoso, J.; Romani, L.; Esperanca, J.; Guedes, H. J. R.; de Sousa, H. C. *Green Chem.* **2004**, *6*, 369−381.

(3) Yasaka, Y.; Wakai, C.; Matubayasi, N.; Nakahara, M. *J. Phys. Chem. A* **2007**, *111*, 541−543.
(4) Bowers, J.; Butts, C. P.; Martin, P. J.; Vergara-Gutierrez, M. C.; Heenan, R. K. *Langmuir* **2004**, *20*, 2191−2198.
(5) Almasy, L.; Turmine, M.; Perera, A. *J. Phys. Chem. B* **2008**, *112*, 2382−2387.
(6) Singh, T.; Kumar, A. *J. Phys. Chem. B* **2007**, *111*, 7843−7851.
(7) Zhu, X.; Wang, Y.; Li, H. R. *AIChE J.* **2009**, *55*, 198−205.
(8) Mele, A.; Tran, C. D.; Lacerda, S. H. D. *Angew. Chem., Int. Ed.* **2003**, *42*, 4364−4366.
(9) Zhao, Y.; Gao, S. J.; Wang, J. J.; Tang, J. M. *J. Phys. Chem. B* **2008**, *112*, 2031−2039.
(10) Remsing, R. C.; Liu, Z. W.; Sergeyev, I.; Moyna, G. *J. Phys. Chem. B* **2008**, *112*, 7363−7369.
(11) Moreno, M.; Castiglione, F.; Mele, A.; Pasqui, C.; Raos, G. *J. Phys. Chem. B* **2008**, *112*, 7826−7836.
(12) Freire, M. G.; Neves, C.; Silva, A. M. S.; Santos, L.; Marrucho, I. M.; Rebelo, L. P. N.; Shah, J. K.; Maginn, E. J.; Coutinho, J. A. P. *J. Phys. Chem. B* **2010**, *114*, 2004−2014.
(13) Wang, Y.; Li, H. R.; Han, S. J. *J. Phys. Chem. B* **2006**, *110*, 24646−24651.
(14) Cammarata, L.; Kazarian, S. G.; Salter, P. A.; Welton, T. *Phys. Chem. Chem. Phys.* **2001**, *3*, 5192−5200.
(15) Koddermann, T.; Wertz, C.; Heintz, A.; Ludwig, R. *Angew. Chem., Int. Edit.* **2006**, *45*, 3697−3702.
(16) Fumino, K.; Wulf, A.; Ludwig, R. *Angew. Chem., Int. Edit.* **2009**, *48*, 3184−3186.
(17) Chang, H. C.; Jiang, J. C.; Liou, Y. C.; Hung, C. H.; Lai, T. Y.; Lin, S. H. *J. Chem. Phys.* **2008**, *129*, 044506.
(18) Lopez-Pastor, M.; Ayora-Canada, M. J.; Valcarcel, M.; Lendl, B. *J. Phys. Chem. B* **2006**, *110*, 10896−10902.
(19) Dominguez-Vidal, A.; Kaun, N.; Ayora-Canada, M. J.; Lendl, B. *J. Phys. Chem. B* **2007**, *111*, 4446−4452.
(20) Zhang, L. Q.; Xu, Z.; Wang, Y.; Li, H. R. *J. Phys. Chem. B* **2008**, *112*, 6411−6419.
(21) Sun, B. J.; Wu, P. Y. *J. Phys. Chem. B* **2010**, *114*, 9209−9219.
(22) Takamuku, T.; Kyoshoin, Y.; Shimomura, T.; Kittaka, S.; Yamaguchi, T. *J. Phys. Chem. B* **2009**, *113*, 10817−10824.
(23) Wu, B.; Zhang, Y. M.; Wang, H. P. *J. Phys. Chem. B* **2009**, *113*, 12332−12336.
(24) Masaki, T.; Nishikawa, K.; Shirota, H. *J. Phys. Chem. B* **2010**, *114*, 6323−6331.
(25) Jeon, Y.; Sung, J.; Kim, D.; Seo, C.; Cheong, H.; Ouchi, Y.; Wawa, R.; Hamaguchi, H. O. *J. Phys. Chem. B* **2008**, *112*, 923−928.
(26) Sarkar, A.; Ali, M.; Baker, G. A.; Tetin, S. Y.; Ruan, Q. Q.; Pandey, S. *J. Phys. Chem. B* **2009**, *113*, 3088−3098.
(27) Hanke, C. G.; Lynden-Bell, R. M. *J. Phys. Chem. B* **2003**, *107*, 10873−10878.
(28) Danten, Y.; Cabaco, M. I.; Besnard, M. *J. Phys. Chem. A* **2009**, *113*, 2873−2889.
(29) Spickermann, C.; Thar, J.; Lehmann, S. B. C.; Zahn, S.; Hunger, J.; Buchner, R.; Hunt, P. A.; Welton, T.; Kirchner, B. *J. Chem. Phys.* **2008**, *129*, 104505.
(30) Mallik, B. S.; Siepmann, J. I. *J. Phys. Chem. B* **2010**, *114*, 12577−12584.
(31) Zahn, S.; Wendler, K.; Delle Site, L.; Kirchner, B. *Phys. Chem. Chem. Phys.* **2011**, *13*, 15083−15093.
(32) Vayssiere, P.; Chaumont, A.; Wipff, G. *Phys. Chem. Chem. Phys.* **2005**, *7*, 124−135.
(33) Schroder, C.; Rudas, T.; Neumayr, G.; Benkner, S.; Steinhauser, O. *J. Chem. Phys.* **2007**, *127*, 234503.
(34) Schroder, C.; Hunger, J.; Stoppa, A.; Buchner, R.; Steinhauser, O. *J. Chem. Phys.* **2008**, *129*, 184501.
(35) Schroder, C.; Neumayr, G.; Steinhauser, O. *J. Chem. Phys.* **2009**, *130*, 194503.
(36) Kelkar, M. S.; Shi, W.; Maginn, E. J. *Ind. Eng. Chem. Res.* **2008**, *47*, 9115−9126.
(37) Kelkar, M. S.; Maginn, E. J. *J. Phys. Chem. B* **2007**, *111*, 4867−4876.
(38) Shi, W.; Maginn, E. J. *J. Phys. Chem. B* **2008**, *112*, 2045−2055.
(39) Jiang, W.; Wang, Y. T.; Voth, G. A. *J. Phys. Chem. B* **2007**, *111*, 4812−4818.
(40) Feng, S.; Voth, G. A. *Fluid Phase Equilib.* **2010**, *294*, 148−156.
(41) Annapureddy, H. V. R.; Hu, Z. H.; Xia, J. C.; Margulis, C. J. *J. Phys. Chem. B* **2008**, *112*, 1770−1776.
(42) Porter, A. R.; Liem, S. Y.; Popelier, P. L. A. *Phys. Chem. Chem. Phys.* **2008**, *10*, 4240−4248.
(43) Picalek, J.; Minofar, B.; Kolafa, J.; Jungwirth, P. *Phys. Chem. Chem. Phys.* **2008**, *10*, 5765−5775.
(44) Raju, S. G.; Balasubramanian, S. *J. Phys. Chem. B* **2009**, *113*, 4799−4806.
(45) Klahn, M.; Stuber, C.; Seduraman, A.; Wu, P. *J. Phys. Chem. B* **2010**, *114*, 2856−2868.
(46) English, N. J.; Mooney, D. A. *Phys. Chem. Chem. Phys.* **2009**, *11*, 9370−9374.
(47) Freire, M. G.; Neves, C.; Shimizu, K.; Bernardes, C. E. S.; Marrucho, I. M.; Coutinho, J. A. P.; Lopes, J. N. C.; Rebelo, L. P. N. *J. Phys. Chem. B* **2010**, *114*, 15925−15934.
(48) Migliorati, V.; Ballirano, P.; Gontrani, L.; Triolo, A.; Caminiti, R. *J. Phys. Chem. B* **2011**, *115*, 4887−4899.
(49) Mendez-Morales, T.; Carrete, J.; Cabeza, O.; Gallego, L. J.; Varela, L. M. *J. Phys. Chem. B* **2011**, *115*, 6995−7008.
(50) Liu, X.; Vlugt, T. J. H.; Bardow, A. *J. Phys. Chem. B* **2011**, *115*, 8506−8517.
(51) Bhargava, B. L.; Klein, M. L. *J. Chem. Theory Comput.* **2010**, *6*, 873−879.
(52) Bhargava, B. L.; Klein, M. L. *Soft Matter* **2009**, *5*, 3475−3480.
(53) Liu, Z. P.; Huang, S. P.; Wang, W. C. *J. Phys. Chem. B* **2004**, *108*, 12978−12989.
(54) Lopes, J. N. C.; Deschamps, J.; Padua, A. A. H. *J. Phys. Chem. B* **2004**, *108*, 2038−2047.
(55) Leskiv, M.; Bernardes, C. E. S.; da Piedade, M. E. M.; Lopes, J. N. C. *J. Phys. Chem. B* **2010**, *114*, 13179−13188.
(56) Bernardes, C. E. S.; da Piedade, M. E. M.; Lopes, J. N. C. *J. Phys. Chem. B* **2011**, *115*, 2067−2074.
(57) Liu, X. M.; Zhang, S. J.; Zhou, G. H.; Wu, G. W.; Yuan, X. L.; Yao, X. Q. *J. Phys. Chem. B* **2006**, *110*, 12062−12071.
(58) Picalek, J.; Kolafa, J. *J. Mol. Liq.* **2007**, *134*, 29−33.
(59) Chaban, V. V.; Voroshylova, I. V.; Kalugin, O. N. *Phys. Chem. Chem. Phys.* **2011**, *13*, 7910−7920.
(60) Esperanca, J.; Lopes, J. N. C.; Tariq, M.; Santos, L.; Magee, J. W.; Rebelo, L. P. N. *J. Chem. Eng. Data* **2010**, *55*, 3−12.
(61) Rocha, M. A. A.; Lima, C.; Gomes, L. R.; Schroder, B.; Coutinho, J. A. P.; Marrucho, I. M.; Esperanca, J.; Rebelo, L. P. N.; Shimizu, K.; Lopes, J. N. C.; Santos, L. *J. Phys. Chem. B* **2011**, *115*, 10919−10926.
(62) Zhong, X. J.; Liu, Z. P.; Cao, D. P. *J. Phys. Chem. B* **2011**, *115*, 10027−10040.
(63) Bhargava, B. L.; Balasubramanian, S. *Chem. Phys. Lett.* **2006**, *417*, 486−491.
(64) Buhl, M.; Chaumont, A.; Schurhammer, R.; Wipff, G. *J. Phys. Chem. B* **2005**, *109*, 18591−18599.
(65) Borodin, O.; Smith, G. D. *J. Phys. Chem. B* **2006**, *110*, 11481−11490.
(66) Borodin, O. *J. Phys. Chem. B* **2009**, *113*, 11463−11478.
(67) Liu, Z. P.; Chen, T.; Bell, A.; Smit, B. *J. Phys. Chem. B* **2010**, *114*, 4572−4582.
(68) Morrow, T. I.; Maginn, E. J. *J. Phys. Chem. B* **2002**, *106*, 12807−12813.
(69) Bhargava, B. L.; Balasubramanian, S. *J. Chem. Phys.* **2007**, *127*, 114510.
(70) Rai, N.; Maginn, E. J. *J. Phys. Chem. Lett.* **2011**, *2*, 1439−1443.
(71) Rai, N.; Maginn, E. J. *Faraday Discuss.* **2012**, *154*, 53−69.
(72) Zhou, Q.; Wang, L. S.; Chen, H. P. *J. Chem. Eng. Data* **2006**, *51*, 905−908.
(73) Malham, I. B.; Letellier, P.; Mayaffre, A.; Turmine, M. *J. Chem. Thermodyn.* **2007**, *39*, 1132−1143.

(74) Malham, I. B.; Turmine, M. *J. Chem. Thermodyn.* **2008**, *40*, 718−723.
(75) Tokuda, H.; Hayamizu, K.; Ishii, K.; Abu Bin Hasan Susan, M.; Watanabe, M. *J. Phys. Chem. B* **2004**, *108*, 16593−16600.
(76) Horn, H. W.; Swope, W. C.; Pitera, J. W.; Madura, J. D.; Dick, T. J.; Hura, G. L.; Head-Gordon, T. *J. Chem. Phys.* **2004**, *120*, 9665−9678.
(77) Jorgensen, W. L.; Jenson, C. *J. Comput. Chem.* **1998**, *19*, 1179−1186.
(78) Martinez, L.; Andrade, R.; Birgin, E. G.; Martinez, J. M. *J. Comput. Chem.* **2009**, *30*, 2157−2164.
(79) Van-Oanh, N. T.; Houriez, C.; Rousseau, B. *Phys. Chem. Chem. Phys.* **2010**, *12*, 930−936.
(80) Plimpton, S. *J. Comput. Phys.* **1995**, *117*, 1−19.
(81) Stoppa, A.; Hunger, J.; Buchner, R. *J. Chem. Eng. Data* **2009**, *54*, 472−479.
(82) Rilo, E.; Pico, J.; Garcia-Garabal, S.; Varela, L. M.; Cabeza, O. *Fluid Phase Equilib.* **2009**, *285*, 83−89.
(83) Swope, W. C.; Andersen, H. C.; Berens, P. H.; Wilson, K. R. *J. Chem. Phys.* **1982**, *76*, 637−649.
(84) Ficke, L. E.; Brennecke, J. F. *J. Phys. Chem. B* **2010**, *114*, 10496−10501.
(85) Sanchez, L. G.; Espel, J. R.; Onink, F.; Meindersma, G. W.; de Haan, A. B. *J. Chem. Eng. Data* **2009**, *54*, 2803−2812.
(86) Schreiner, C.; Zugmann, S.; Hartl, R.; Gores, H. J. *J. Chem. Eng. Data* **2010**, *55*, 1784−1788.
(87) Wang, J. J.; Tian, Y.; Zhao, Y.; Zhuo, K. *Green Chem.* **2003**, *5*, 618−622.
(88) Cadena, C.; Zhao, Q.; Snurr, R. Q.; Maginn, E. J. *J. Phys. Chem. B* **2006**, *110*, 2821−2832.
(89) Huang, X. H.; Margulis, C. J.; Li, Y. H.; Berne, B. J. *J. Am. Chem. Soc.* **2005**, *127*, 17842−17851.
(90) Su, W. C.; Chou, C. H.; Wong, D. S. H.; Li, M. H. *Fluid Phase Equilib.* **2007**, *252*, 74−78.
(91) Wong, C. L.; Soriano, A. N.; Li, M. H. *Fluid Phase Equilib.* **2008**, *271*, 43−52.
(92) Sarraute, S.; Gomes, M. F. C.; Padua, A. A. H. *J. Chem. Eng. Data* **2009**, *54*, 2389−2394.
(93) Koddermann, T.; Ludwig, R.; Paschek, D. *ChemPhysChem* **2008**, *9*, 1851−1858.
(94) Hayamizu, K.; Tsuzuki, S.; Seki, S.; Fujii, K.; Suenaga, M.; Umebayashi, Y. *J. Chem. Phys.* **2010**, *133*, 194505.